blood®
Regular Article

IMMUNOBIOLOGY AND IMMUNOTHERAPY

Cereblon harnesses Myc-dependent bioenergetics and activity of CD8$^+$ T lymphocytes

Rebecca S. Hesterberg,[1,2,*] Matthew S. Beatty,[1,*] Ying Han,[1,3,*] Mario R. Fernandez,[4] Afua A. Akuffo,[1,2] William E. Goodheart,[1] Chunying Yang,[4] Shiun Chang,[1,2] Christelle M. Colin,[1] Aileen Y. Alontaga,[1] Jessica M. McDaniel,[1] Adam W. Mailloux,[1] Julia M. R. Billington,[1,2] Lanzhu Yue,[1,5] Shonagh Russell,[2,6] Robert J. Gillies,[6] Sang Y. Yun,[7] Muhammad Ayaz,[7] Nicholas J. Lawrence,[8] Harshani R. Lawrence,[7] Xue-Zhong Yu,[9] Jianing Fu,[9] Lancia N. Darville,[10] John M. Koomen,[10,11] Xiubao Ren,[3] Jane Messina,[12] Kun Jiang,[12] Timothy J. Garrett,[13] Anjali M. Rajadhyaksha,[14,15] John L. Cleveland,[4] and Pearlie K. Epling-Burnette[1]

[1]Department of Immunology, Moffitt Cancer Center and Research Institute, Tampa, FL; [2]Cancer Biology PhD Program, University of South Florida, Tampa, FL; [3]Department of Immunology, Tianjin Cancer Institute and Hospital, Tianjin Medical University, Tianjin, China; [4]Department of Tumor Biology, Moffitt Cancer Center and Research Institute, Tampa, FL; [5]Department of Hematology, Tianjin Medical University General Hospital, Tianjin, China; [6]Department of Cancer Physiology, [7]Chemical Biology Core, and [8]Department of Drug Discovery, Moffitt Cancer Center and Research Institute, Tampa, FL; [9]Department of Microbiology and Immunology, Medical University of South Carolina, Charleston, SC; [10]Proteomics and Metabolomics Core, [11]Department of Molecular Oncology, and [12]Department of Anatomic Pathology and Cutaneous Oncology, Moffitt Cancer Center and Research Institute, Tampa, FL; [13]Department of Pathology, Immunology, and Laboratory Medicine, University of Florida, Gainesville, FL; and [14]Pediatric Neurology, Pediatrics, Weill Family Brain and Mind Research Institute, and [15]Graduate Program in Neuroscience, Weill Cornell Medical College, Cornell University, Cornell, NY

KEY POINTS

- **Cereblon loss or treatment with cereblon E3 ligase-modulating compounds provokes a hypermetabolic T-cell effector phenotype.**
- **Nutrient consumption and metabolism of activated CD8$^+$ T cells is orchestrated by cereblon's control of Myc.**

Immunomodulatory drugs, such as thalidomide and related compounds, potentiate T-cell effector functions. Cereblon (CRBN), a substrate receptor of the DDB1-cullin-RING E3 ubiquitin ligase complex, is the only molecular target for this drug class, where drug-induced, ubiquitin-dependent degradation of known "neosubstrates," such as IKAROS, AIOLOS, and CK1α, accounts for their biological activity. Far less clear is whether these CRBN E3 ligase-modulating compounds disrupt the endogenous functions of CRBN. We report that CRBN functions in a feedback loop that harnesses antigen-specific CD8$^+$ T-cell effector responses. Specifically, *Crbn* deficiency in murine CD8$^+$ T cells augments their central metabolism manifested as elevated bioenergetics, with supraphysiological levels of polyamines, secondary to enhanced glucose and amino acid transport, and with increased expression of metabolic enzymes, including the polyamine biosynthetic enzyme ornithine decarboxylase. Treatment with CRBN-modulating compounds similarly augments central metabolism of human CD8$^+$ T cells. Notably, the metabolic control of CD8$^+$ T cells by modulating compounds or *Crbn* deficiency is linked to increased and sustained expression of the master metabolic regulator MYC. Finally, *Crbn*-deficient T cells have augmented antigen-specific cytolytic activity vs melanoma tumor cells, ex vivo and in vivo, and drive accelerated and highly aggressive graft-versus-host disease. Therefore, CRBN functions to harness the activation of CD8$^+$ T cells, and this phenotype can be exploited by treatment with drugs. (*Blood*. 2020;136(7):857-870)

Introduction

Cereblon (CRBN), first discovered through genetic linkage analysis in patients who had a mild, autosomal recessive, non-syndromic intellectual disability, is the sole documented target of a thalidomide-derived class of E3 ligase-modulating agents that induce immune modulation, teratogenicity, and antineoplastic activity[1,2] in multiple myeloma,[3,4] B-cell malignancies,[5-7] and deletion chromosome 5q myelodysplastic syndrome.[8,9] CRBN functions as the substrate-recruiting module for DDB1 (DNA damage-binding protein-1), Cul4A or B (cullin 4), and ROC1 (regulator of cullin 1) E3 ubiquitin ligase complex,[10-12] and binding of immune modulating compounds (hereinafter referred to as IM) alters the specificity of this E3 ligase, to degrade a cast of "neosubstrate" proteins that play important roles in hematopoiesis, angiogenesis, and T- and NK-cell regulation.[6,13-15] Of these known targets, the lymphocyte transcriptional repressor IKAROS[16] and its paralogue AIOLOS[17] are the only suggested determinants of IM compound-driven T-cell phenotypes,[14,18] However, it has been suggested that some of the IM properties of these compounds reflect displacement of normal CRBN binding partners, which are poorly characterized.[19] In particular, *Crbn*-deficient CD4$^+$ T cells augment disease pathogenesis in a model of experimental autoimmune encephalomyelitis; this has been attributed to epigenetic regulation of the *Kcna3* gene, which encodes Kv1.3, a voltage-activated potassium ion channel.[20]

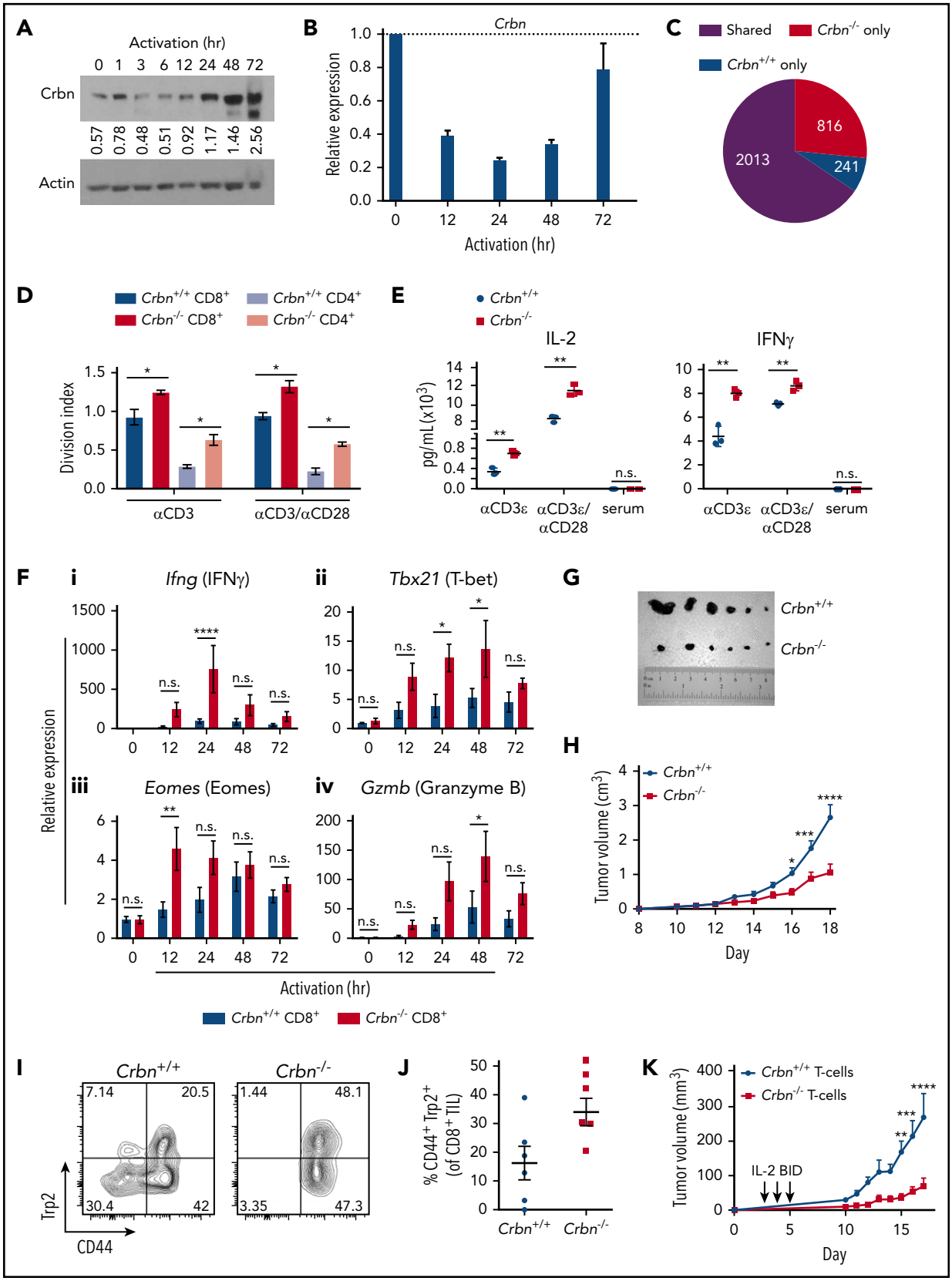

Figure 1. Ablation of *Crbn* augments T-cell activation and function. CRBN protein (A) and mRNA (B) levels following anti-CD3ε/anti-CD28 stimulation of mouse (C57Bl/6) T cells. (C) Number of transcriptional changes after anti-CD3ε+anti-CD28 stimulation of $Crbn^{+/+}$ T cells, $Crbn^{-/-}$ T cells, or both (Shared). (D) $Crbn^{+/+}$ and $Crbn^{-/-}$ CD4$^+$ and CD8$^+$ T-cell proliferation after 72 hours of 5 μg/mL anti-CD3ε$^{+/-}$/1 μg/mL anti-CD28 stimulation, as measured by CellTrace Violet (CTV), quantified by the division index (mean number of divisions per cell). (E) Production of IL-2 and IFN-γ after 72 hours of activation in $Crbn^{+/+}$ and $Crbn^{-/-}$ T cells after stimulation with anti-CD3ε$^{+/-}$/anti-CD28. (F) Fold change in levels of the indicated mRNAs (determined by qRT-PCR) after activation of $Crbn^{+/+}$ and $Crbn^{-/-}$ CD8$^+$ T cells for 12, 24, 48, and 72 hours, relative to levels of

T-cell stimulation leads to dynamic changes in metabolic programming that are critical for the survival and homeostasis of the T-cell compartment,[21] and T cells must elevate both aerobic glycolysis and oxidative phosphorylation (OXPHOS), to promote antigen-induced growth, proliferation, and effector functions.[22-24] Thus, identifying T-cell metabolic regulators, especially those targetable by small-molecule agonists or inhibitors, is likely to have a dramatic impact on various forms of immunotherapy.[25] With a focus on $CD8^+$ T cells, we report that CRBN expression is dynamically regulated during T-cell receptor (TCR) activation, CRBN controls expression of the master T-cell metabolic regulator c-MYC (MYC),[26] and *Crbn* deficiency or IM compound treatment confers a unique and superior T-cell metabolic program. Collectively, these findings reveal CRBN to be a tractable regulator of T-cell metabolism and function that has broad potential to modulate T-cell effector (T_E) functions in clinical settings.

Methods

A summary of all key resources is provided in supplemental Table 1, and detailed methods are provided in supplemental Material and supplemental Tables 2 and 3, available on the *Blood* Web site.

T-cell isolation and activation

Spleens from 6- to 12-week-old mice were processed into single-cell suspensions and placed in red blood cell lysis buffer for 1 minute. $CD3^+$, $CD8^+$, and $CD4^+$ T and B cells were isolated by immunomagnetic negative selection according to the manufacturer's protocol (Miltenyi Biotec, Bergisch Gladbach, Germany). Human T cells were derived from buffy coats (OneBlood, Tampa, FL) and were isolated per the manufacturer's protocol and frozen at −80°C in 90% fetal bovine serum and 10% dimethyl sulfoxide before use. Before activation, T cells were rested in complete medium for 1 to 3 hours at 37°C. For flow-based assays, reverse transcription-polymerase chain reaction (RT-PCR), Seahorse analyses, cytokine analysis, and metabolomics, 96-well round bottom plates were coated with 3 to 5 μg/mL anti-CD3 in 100 μL phosphate-buffered saline overnight at 4°C or for 90 minutes at 37°C. $Crbn^{+/+}$ and $Crbn^{-/-}$ T cells were plated in equal numbers (2×10^5 per well), with and without 1 μg/mL anti-CD28. For western blot analysis, 12-well plates were similarly coated, and 2×10^6 T cells per well were plated with 1 μg/mL anti-CD28. For OT1 and OT1;$Crbn^{-/-}$ activation, 10^6 splenocytes were plated per well in a 24-well plate with 0.001 to 1.0 nM peptide and 10 ng/mL interleukin-2 (IL-2), unless otherwise indicated.

Experimental melanoma mouse model and adoptive cell transfer

Mice were injected subcutaneously with 10^5 B16 melanoma cells on the left flank. Tumors were measured every 2 to 3 days by 2 perpendicular measurements, and volume was calculated by the equation $axb^2 \times 0.52$, where *a* is the longest measurement and *b* is the perpendicular measurement. Mice were euthanized when tumors ulcerated or the longest side exceeded 20 mm. Some cohorts of mice were euthanized early (days 10-14) for tumor-infiltrating lymphocyte analysis. Tumors were processed into a single-cell suspension and agitated for 30 minutes in complete RPMI medium supplemented with collagenase I and IV, hyaluronidase, and DNase I. Populations of T cells from tumors were stained for flow cytometry and immediately analyzed. For adoptive cell transfer, CD45.1 mice were sublethally irradiated for 3 days after initial tumor inoculation at 600 rad, and 2×10^6 T cells were injected via tail vein. The mice were then treated with 250 000 IU IL-2 via intraperitoneal injection twice daily for 3 days.

Experimental GVHD mouse model

To induce graft-versus-host disease (GVHD), we performed the major histocompatibility complex–mismatched C57BL/6-to-BALBc/J bone marrow transplantation model. $Crbn^{-/-}$ and $Crbn^{+/+}$ T cells were purified according to the manufacturer's instructions (EasySep). BALB/c mice were lethally irradiated with 800 to 900 cGy and injected with 5×10^6 CD3-depleted $Crbn^{+/+}$ bone marrow cells, with and without 10^6 T cells from either $Crbn^{+/+}$ or $Crbn^{-/-}$ mice via the tail vein 24 hours after irradiation. Weight was measured at various intervals. Interferon-γ (IFN-γ) and IL-17 were measured by flow cytometry in splenocytes harvested 14 days after transplantation and restimulated with phorbol myristate acetate, ionomycin, and 1 μL/mL brefeldin A.

Results

CRBN is dispensable for T-cell development but represses $CD8^+$ T-cell activation

First, we assessed the effects of TCR activation with anti-CD3ε/anti-CD28 on CRBN expression in both mouse and primary human $CD8^+$ T cells. Quantitative RT-PCR (qRT-PCR) and immunoblot analyses revealed that CRBN expression was dynamically controlled in activated T cells, where (1) there were marked reductions in levels of CRBN protein (Figure 1A) and messenger RNA (mRNA; Figure 1B) in mouse and human T cells (supplemental Figure 1A) immediately after TCR activation; and (2) *Crbn* mRNA expression then rebounded, and CRBN protein levels rose to levels higher than those found in unstimulated T cells. These findings suggest that CRBN functions in controlling T-cell activation. Indeed, expression-profiling analysis of unstimulated vs anti-CD3ε/anti-CD28–activated $Crbn^{+/+}$ and $Crbn^{-/-}$ $CD3^+$ T cells revealed that, although there were few differences in gene expression in unstimulated T cells, there were 816 differentially expressed genes in activated $Crbn^{-/-}$ T cells (Figure 1C; supplemental Figure 1B).

To test the effects of Crbn on T-cell phenotypes, we assessed *Crbn*-deficient mice,[27] where Crbn expression is abolished in all tissues (supplemental Figure 1C-D).[27] Consistent with a previous

Figure 1 (continued) *B2M* (β_2-microglobulin) mRNA: *Ifng* (i), *Tbx21* (ii), *Eomes* (iii), and *Gzmb* (iv). (G) Images of representative B16 melanoma tumors in $Crbn^{+/+}$ and $Crbn^{-/-}$ recipient mice and (H) tumor growth over time in these 2 cohorts. (I-J) CD44 cell surface expression and Trp2-peptide reactivity of CD8 tumor-infiltrating lymphocytes from B16 tumor-bearing $Crbn^{+/+}$ and $Crbn^{-/-}$ mice (day 10). (K) Tumor growth of B16 tumor-bearing mice after adoptive cell transfer of $Crbn^{+/+}$ and $Crbn^{-/-}$ T cells and treatment with IL-2 twice a day (arrows). All results are representative of at least 2 independent experiments in at least 3 mice (excluding microarray analysis). n.s., not significant; $^*P < .05$; $^{**}P < .01$; $^{***}P < .001$; $^{****}P < .0001$.

report of mice with a similar global deletion of *Crbn*,[20] splenic CD4$^+$ and CD8$^+$ T-cell populations were equally distributed in *Crbn*$^{-/-}$ and *Crbn*$^{+/+}$ littermates (supplemental Figure 1E), which had similar proportions of CD69$^+$ and CD25$^+$ T cells in the spleen, lymph node, peripheral blood, and bone marrow (supplemental Table 4). The distribution of naïve, long-term memory T cells (T_M) and effector T_M cells was also comparable in 3-month-old C*rbn*$^{-/-}$ and C*rbn*$^{+/+}$ littermates, and the counts of thymocytes and thymic subpopulations were similar in C*rbn*$^{-/-}$ and *Crbn*$^{+/+}$ mice (supplemental Table 4). *Crbn* deficiency also had no effect on the distribution of splenic B cells, NK cells, or regulatory T cells (Tregs) (supplemental Table 4). Finally, homeostatic responses within the T-cell compartment were similar in studies evaluating age-associated T-cell phenotypes, where *Crbn*$^{-/-}$ and *Crbn*$^{+/+}$ mice have similar proportions of activated CD44$^+$CD8$^+$ and CD44$^+$CD4$^+$ T cells (supplemental Figure 1F) and the expected age-dependent increases in CD44$^+$ cells that are induced by homeostatic turnover.[28,29]

To assess the possible effects of *Crbn* deficiency on T-cell activation, *Crbn*$^{-/-}$ and *Crbn*$^{+/+}$ T cells were stimulated with increasing concentrations of anti-CD3ε, with or without anti-CD28 costimulation. Notably, there were marked increases in the average number of divisions of CD4$^+$ and CD8$^+$ C*rbn*$^{-/-}$ T cells based on CellTrace Violet staining after activation with anti-CD3ε and even without anti-CD28 costimulation (Figure 1D). Strikingly, increases in the cytokines IL-2 and IFN-γ (Figure 1E) were detected with and without CD28 costimulation, although serum levels of the cytokines were not detected in *Crbn*$^{-/-}$ mice. Finally, TNF-α, IL-17, and IL-10 levels were also increased in anti-CD3ε stimulated *Crbn*$^{-/-}$ T cells, but no differences were detected in IL-4 levels (supplemental Figure 1G).

To assess whether the hyperproliferative state of *Crbn*$^{-/-}$ T cells is associated with changes in the levels of neosubstrates of Crbn (Ikaros and CK1α) or transcription targets of Ikaros (ie, Irf-4), western blot analyses were performed in activated *Crbn*$^{+/+}$ and *Crbn*$^{-/-}$ T cells. Although Ikaros, CK1α, and particularly, Irf-4, were induced after TCR stimulation, their expression levels were not dependent upon *Crbn* status (supplemental Figure 1H). Moreover, *Ikzf1* mRNA levels were not *Crbn* related (supplemental Figure 1I).

To determine if *Crbn* deficiency augments CD8$^+$ T_E function and activates *Crbn*$^{-/-}$ and *Crbn*$^{+/+}$, CD8$^+$ T cells were assessed for effector markers after TCR stimulation.[30,31] Interestingly, activated *Crbn*$^{-/-}$ CD8$^+$ T cells had significant increases in T_E signature genes, including IFN-γ (*Ifng*), T-bet (T-box 21, *Tbx21*), *Eomes*, and granzyme B (*Gzmb*) (Figure 1F) and perforin (*Prf1*) (supplemental Figure 1J).

To determine if *Crbn*$^{-/-}$ CD8+ T cells had increased effector function in vivo, we assessed their activity in syngeneic B16 melanoma transplantation studies. As recipients, *Crbn*$^{-/-}$ mice demonstrated a significant reduction in tumor progression and burden vs *Crbn*$^{+/+}$ mice (Figure 1G-H) and had and an increased number of CD44$^+$ melanoma antigen tyrosinase–related protein (Trp2)–reactive CD8$^+$ tumor-infiltrating lymphocytes (Figure 1I-J). Notably, adoptive cell-transfer studies of *Crbn*$^{-/-}$ vs *Crbn*$^{+/+}$ T cells into B16 melanoma-bearing mice demonstrated that Crbn deficiency confers superior antitumor activity in T cells (Figure 1K). Thus, *Crbn* deficiency promotes a hyperactive and superior T_E phenotype.

CRBN controls the bioenergetics of activated T cells

CD4$^+$ *Crbn*$^{-/-}$ T cells have a hyperactivated response after TCR stimulation that is associated with increased expression of the potassium channel Kv1.3.[20] We confirmed this finding but, interestingly, activated *Crbn*$^{-/-}$ CD8$^+$ T cells displayed decreases in *Kcna3* mRNA levels compared with activated *Crbn*$^{+/+}$ CD8$^+$ T cells (Figure 2A). Thus, other mechanisms likely account for the hyperactivated phenotype of *Crbn*$^{-/-}$ CD8$^+$ T cells.

To gain insight into the hyperactivated state manifested in *Crbn*$^{-/-}$ CD8$^+$ T cells, gene set enrichment analysis (GSEA) was performed on transcripts unique to activated *Crbn*$^{-/-}$ T cells (Figure 1D). This analysis revealed an enrichment for metabolic and mitochondrial processes (Figure 2B). Consistent with these findings, anti-CD3ε+anti-CD28–activated *Crbn*$^{-/-}$ CD8$^+$ T cells had higher basal rates of glycolysis and respiration than activated *Crbn*$^{+/+}$ T cells, based on their extracellular acidification rates (ECARs; Figure 2C; supplemental Figure 2) and oxygen consumption rates (OCR; Figure 2D; supplemental Figure 2).

Costimulation with CD28 or other costimulatory molecules is normally necessary to induce robust changes in T-cell metabolism.[32] However, increases in basal ECAR and OCR were also evident in polyclonal *Crbn*$^{-/-}$ CD8$^+$ T cells stimulated with anti-CD3ε alone (Figure 2C-D). Further, the overall reduction in OCR observed after oligomycin treatment (which suppresses mitochondrial adenosine triphosphatase) indicated that mitochondrial adenosine triphosphate (ATP) production rates were elevated in *Crbn*$^{-/-}$ vs *Crbn*$^{+/+}$ CD8$^+$ T cells (supplemental Figure 2). Interestingly, Activated CD8$^+$ *Crbn*$^{-/-}$ T cells displayed significant increases in glucose uptake (as measured by uptake of the fluorescent glucose analogue 2-NBDG; Figure 2E-F), marked increases in hexokinase activity (Figure 2G), and a higher ratio of the oxidized and reduced forms of nicotinamide adenine dinucleotide (NAD$^+$/NADH; Figure 2H), which is consistent with robust respiration and glycolytic rates.[33] Static levels of intracellular ATP were comparable in activated *Crbn*$^{-/-}$ and *Crbn*$^{+/+}$ T cells, however, suggesting that the generation of ATP is proportional to its utilization (Figure 2I). Finally, treatment with 2-deoxyglucose, which blocks glycolysis, abolished the proliferative advantage of activated *Crbn*$^{-/-}$ T cells (Figure 2J). Thus, glycolysis is necessary for the robust metabolic phenotype of *Crbn*$^{-/-}$ CD8$^+$ T cells and contributes to their superior proliferative response.

Crbn controls antigen-specific activation of CD8$^+$ effector function

To assess the role of Crbn in antigen-specific activation we evaluated TCR signal strength, spontaneous activation, and persistence in antigen-activated *Crbn*$^{-/-}$ CD8$^+$ T cells, which were generated by crossing *Crbn*$^{-/-}$ mice with ovalbumin (OVA) peptide TCR-transgenic mice (OT1).[34] As expected, 96% of CD8$^+$ splenocytes from *Crbn*$^{-/-}$;OT-1 mice displayed reactivity to the H-2K^b OVA tetramer (Figure 3A). In these experiments, splenocytes were stimulated with the immunodominant, high-affinity SIINFEKL peptide (N4); with a variant, intermediate-affinity OVA peptide (SAINFEKL, A2); or with an OVA peptide (SIIGFEKL, G4) that has very low affinity for the OT1 TCR.[35] After

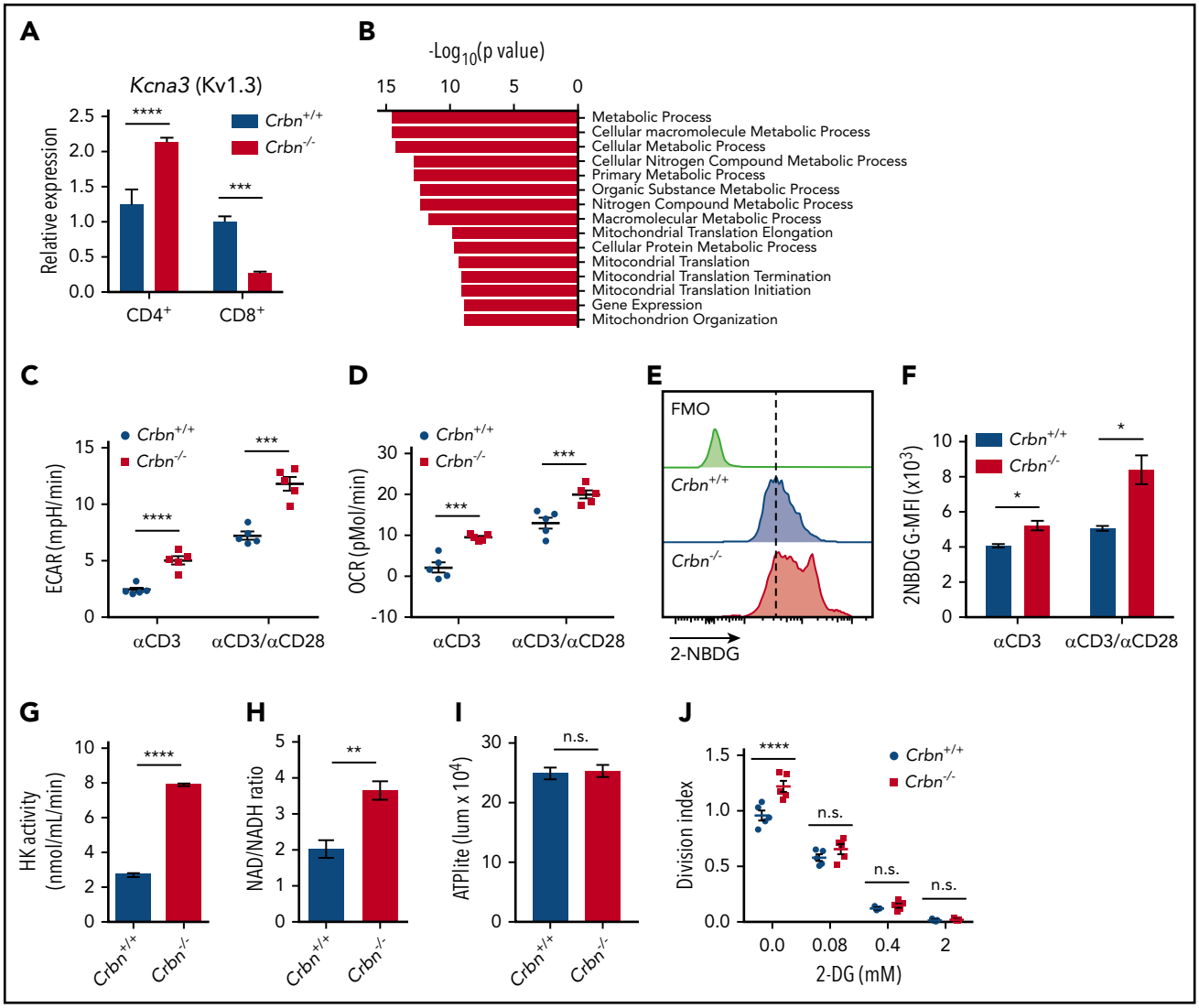

Figure 2. CRBN loss augments energetics of activated CD8⁺ T cells. (A) Relative expression of *Kcna3* (vs *B2M*) after a 24-hour stimulation of *Crbn*$^{+/+}$ and *Crbn*$^{-/-}$ CD4⁺ and CD8⁺ T cells with anti-CD3ε, with or without anti-CD28. (B) Pathway analysis of transcripts that specifically change in activated *Crbn*$^{-/-}$ T cells (Figure 1D). Basal ECARs (C) and OCRs (D) in anti-CD3ε, with or without anti-CD28–activated *Crbn*$^{+/+}$ and *Crbn*$^{-/-}$ CD8⁺ T cells. (E-F) Glucose uptake of activated *Crbn*$^{+/+}$ and *Crbn*$^{-/-}$ CD8⁺ T cells with anti-CD3ε, with or without anti-CD28, as measured by the fluorescent glucose analogue 2-NBDG; G-MFI, geometric MFI; FMO, fluorescence −1. (G) Hexokinase (HK) enzymatic activity of activated *Crbn*$^{+/+}$ and *Crbn*$^{-/-}$ CD8⁺ T cells. (H) NAD⁺/NADH ratio of activated *Crbn*$^{+/+}$ and *Crbn*$^{-/-}$ CD8⁺ T cells. (I) ATP production of activated *Crbn*$^{+/+}$ and *Crbn*$^{-/-}$ CD8⁺ T cells. (J) *Crbn*$^{+/+}$ and *Crbn*$^{-/-}$ CD8⁺ T-cell proliferation after 72 hours of anti-CD3ε+anti-CD28 stimulation with 2-deoxyglucose to suppress glycolysis. All results are representative of at least 2 independent experiments. n.s., not significant; * $P < .05$; ** $P < .01$; *** $P < .001$; **** $P < .0001$.

72 hours of activation with the N4 and A2 peptides, CD69 was elevated in OT1;*Crbn*$^{-/-}$ T cells (Figure 3B) independent of exogenous IL-2 (Figure 3C). In contrast, there was no response to the G4 peptide or to the OT1-irrelevant Trp2 peptide (Figure 3B-C). Interestingly, OT1 and OT1;*Crbn*$^{-/-}$ T cells expressed comparable levels of CD69 in response to the N4 and A2 peptides immediately after activation, but prolonged elevated expression of CD69 manifested in OT1;*Crbn*$^{-/-}$ T cells (Figure 3D). The proliferation of OT1;*Crbn*$^{-/-}$ T cells was also augmented in response to increasing doses of N4 and A2 peptides when compared to OT1 T cells; but again, OT1;*Crbn*$^{-/-}$ T cells did not respond to the low-affinity G4 peptide (Figure 3E). Thus, CRBN controls the persistence of activated T cells after antigen stimulation, but does not confer responses to a very-low-affinity or irrelevant antigen. In accordance with these findings, peptide-stimulated OT1;*Crbn*$^{-/-}$ CD8⁺ T cells had superior viability and higher basal ECAR, basal OCR, and cytotoxic potential against an OVA-expressing B16 melanoma tumor target (Figure 3G-I) and increased uptake of the glucose analogue 2-NBDG (Figure 3J-K).

CRBN harnesses arginine and glutamine metabolism to control polyamine levels

Aerobic glycolysis is a well-known regulator of the CD8⁺ T_E phenotype.[36,37] To assess mechanisms that may account for the superior effector phenotype of *Crbn*$^{-/-}$ CD8⁺ T cells, we performed global metabolomic profiling by liquid chromatography-mass spectrometry (LC-MS), in both positive and negative ionization modes. MZmine (freeware) was used to identify and align features of activated *Crbn*$^{+/+}$ and *Crbn*$^{-/-}$ CD8⁺ T cells, which were then defined by principal component analysis. Finally, those with a twofold or greater change and $P \leq .1$ were

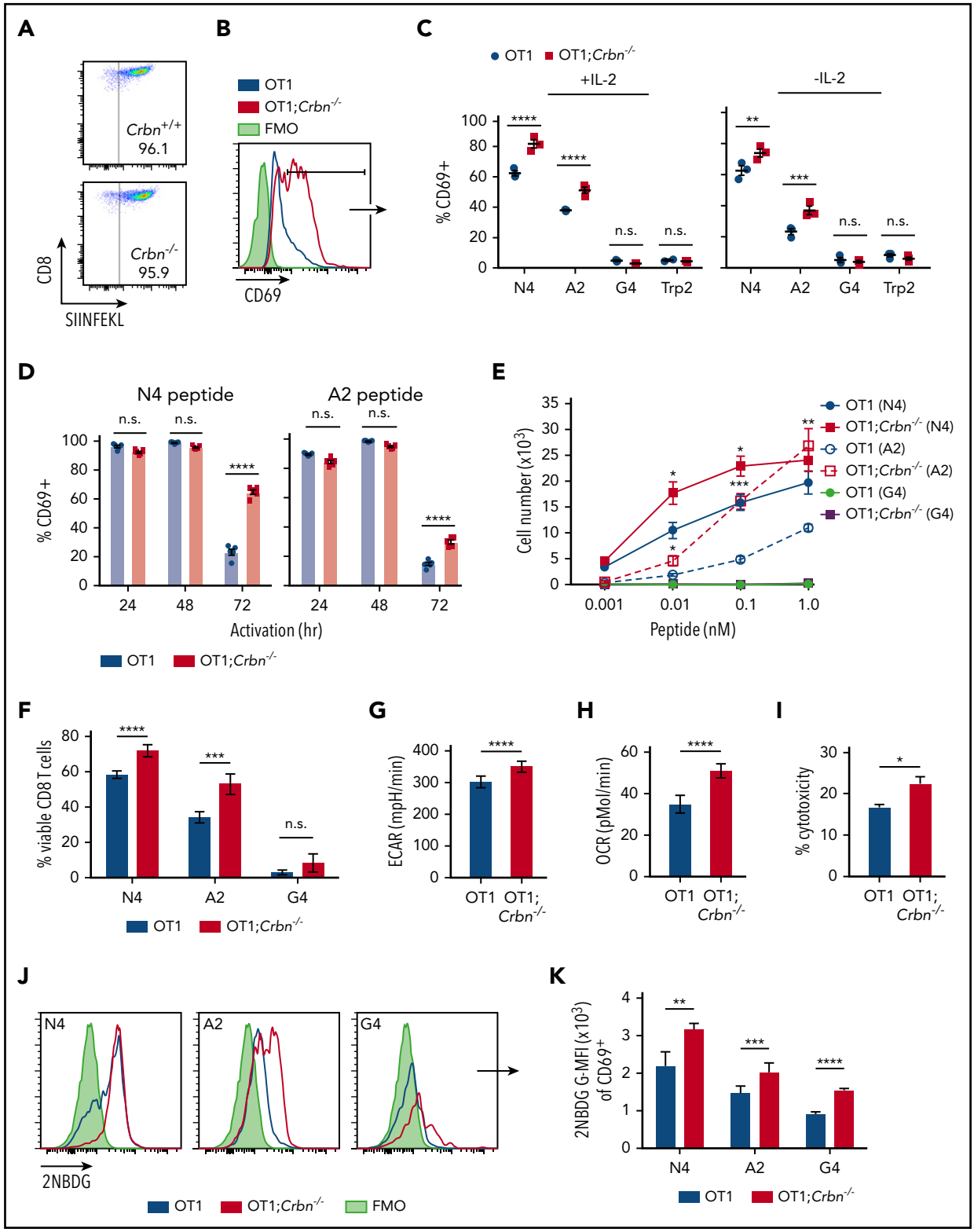

Figure 3. CRBN controls antigen-specific CD8⁺ T-cell activation. (A) OVA-reacting, tetramer-positive CD8⁺ splenocytes from OT1 and OT1;*Crbn*$^{-/-}$ mice. (B-C) Total number of CD69-expressing OT1 and OT1;*Crbn*$^{-/-}$ T cells at 72 hours in response to SIINFEKL (N4, B), or in response to N4, SAINFEKL (A2), SIIGFEKL (G4), or Trp2 peptides, with or without added IL-2 (C). (D) CD69 expression in OT1 and OT1;*Crbn*$^{-/-}$ T cells after 24, 49, and 72 hours of culture with 0.1 nM N4 or A2 peptide. (E) Dose response of peptide-reactive T cells with 0.1 nM of N4, A2, or G4 peptide stimulation, as determined by cell counting. (F) Percentage of viable CD8⁺ T cells after stimulation with the N4, A2, and G4 peptides for 72 hours. Basal ECARs (G) and basal OCRs (H) from OT1 and OT1;*Crbn*$^{-/-}$ CD8⁺ T cells stimulated with SIINFEKL peptide for 24 hours. (I) Percentage of cytotoxicity of OT1 and OT1;*Crbn*$^{-/-}$ T cells vs OVA-expressing B16 cells (72-hour coculture). (J) Flow analysis of glucose uptake based on fluorescent glucose analogue, 2-NBDG;G-MFI, after 48 hours of activation with the N4, A2, and G4 peptides of OT1 and OT1;*Crbn*$^{-/-}$ T cells in CD69⁺ cells. (K) Summary of data shown in panel J. All results are representative of at least 2 independent experiments. n.s., not significant, $*P < .05$; $**P < .01$; $***P < .001$; $****P < .0001$.

analyzed for pathway overrepresentation (supplemental Figure 3A-B). Pathway enrichment analysis revealed highly significant involvement of the arginine/proline pathway (supplemental Figure 3A; false discovery rate [FDR], 0.006; −log(p), 9.47). A heatmap of metabolites detected in this pathway suggested that activated *Crbn*$^{-/-}$ CD8$^+$ T cells have increased utilization of glutamine, arginine, and ornithine, as these cells had markedly elevated levels of downstream metabolites, including proline, putrescine, *N*-acetyl putrescine, 4-acetamidobutanoic acid, and the longer chain polyamines spermidine and spermine (Figure 4A-B; supplemental Figure 3C).

Both L-arginine (L-Arg) and L-glutamine (L-Gln) can serve as the carbon and nitrogen units for polyamine biosynthesis,[38] and L-Gln transporters are needed to sustain glutaminolysis in T cells.[26] Notably, activated *Crbn*$^{-/-}$ CD8$^+$ T cells expressed elevated levels of *Slc7a1* encoding the L-Arg transporter CAT-1,[39] and the *Slc38a1* (SNAT1) and *Slc1a5* (ASCT2) L-Gln transporters,[40] compared with activated wild-type CD8$^+$ T cells (Figure 4B; supplemental Figure 3D-E). Moreover, elevated levels of mRNAs encoding enzymes that catabolize ornithine or direct polyamine biosynthesis, specifically *Odc1*, *Oat*, *Srm*, and *Sms*, confirmed that this pathway is amplified in activated *Crbn*$^{-/-}$ vs *Crbn*$^{+/+}$ CD8$^+$ T cells (Figure 4B; supplemental Figure 3G-J). Further, uptake studies of U-^{14}C-labeled L-Arg and L-Gln confirmed transport of both amino acids is enhanced in activated *Crbn*$^{-/-}$ CD8$^+$ T cells (Figure 4C), and targeted tandem mass spectrometry (LC-MS/MS) analyses confirmed that activated *Crbn*$^{-/-}$ T cells have supraphysiological intracellular levels of putrescine, spermidine, and spermine (Figure 4D). Expression of CD98/Slc3A2, which forms a heterodimer with Slc7A5, to direct transport of neutral branched-chain amino acids,[41] was also significantly elevated in *Crbn*$^{-/-}$ CD8$^+$ T cells (Figure 4E). Finally, the hyperproliferative state of activated *Crbn*$^{-/-}$ CD8$^+$ T cells required increases in polyamines, as this was abolished by cotreatment with α-difluoromethylornithine, an irreversible inhibitor of ODC[42] (Figure 4F).

Superior T_E phenotypes of *Crbn*$^{-/-}$ CD8$^+$ T cells appear to be largely caused by increases in glycolysis and OXPHOS fueled by enhanced nutrient availability and metabolism, yet there was a trend toward higher spare respiratory capacity in activated *Crbn*$^{-/-}$ CD8$^+$ T cells (supplemental Figures 2D and 3K). Although OXPHOS is necessary for energy generation in T_E cells, spare respiratory capacity is considered an important driver for T_M differentiation, and mitochondrial remodeling appears to instruct T-cell metabolic programming where T_Ms manifest fused mitochondria.[21] Mitochondrial biomass and mitochondrial membrane potential were not significantly different in activated *Crbn*$^{-/-}$ and *Crbn*$^{+/+}$ CD8$^+$ T cells (supplemental Figure 3L-M), yet transmission electron microscopy revealed modest increases in the number of mitochondria in activated *Crbn*$^{-/-}$ cells (supplemental Figure 3N-O). However, mitochondrial length and superoxide reactive oxygen species (supplemental Figure 3P-Q) were similar in *Crbn*$^{+/+}$ and *Crbn*$^{-/-}$ CD8$^+$ T cells, which may reflect increased glutathione metabolism in *Crbn*$^{-/-}$ CD8$^+$ T cells (supplemental Figure 3A). Finally, treatment with the ATP-synthase inhibitor oligomycin[43] also impaired the proliferative advantage of activated *Crbn*$^{-/-}$ T cells (Figure 4G). Thus, nutrients that fuel both glycolysis and OXPHOS contribute to the superior response of *Crbn*$^{-/-}$ CD8$^+$ T cells that aligns both genetically and metabolically with a T_E phenotype.

A CRBN-Myc circuit controls CD8$^+$ T-cell effector phenotypes and metabolism

To elucidate the precise pathway activated in *Crbn*$^{-/-}$ T cells, we subjected differentially expressed genes (Figure 2A) to GSEA for transcriptional drivers. These analyses revealed that the gene expression changes in activated *Crbn*$^{-/-}$ T cells largely reflect differences in Myc:Max and Myc transcription targets (supplemental Figure 4A; FDR q = 0.002). Consistent with this hypothesis, there were significant increases and sustained levels of Myc protein in activated *Crbn*$^{-/-}$ vs *Crbn*$^{+/+}$ total T cells and of *Myc* mRNA in activated *Crbn*$^{-/-}$ vs *Crbn*$^{+/+}$ CD8$^+$ T cells (Figure 5A-B). Myc is a master regulator of metabolic transcription programs[44] and induces polyamine biosynthesis[45] via transcriptional induction of *Odc1*, which is elevated in *Crbn*$^{-/-}$ T cells (Figure 3B; supplemental Figure 3G). Further, in activated T cells, Myc induces the expression of transporters and enzymes that direct glutamine catabolism and flux into polyamines,[26,38,45] and provokes increases in cell size. Interestingly, *Crbn*$^{-/-}$ CD8$^+$ T cells were significantly larger, based on forward scatter area, compared with *Crbn*$^{+/+}$ CD8$^+$ T cells (supplemental Figure 4B).

Given these phenotypes, to assess whether the superior metabolic phenotype of *Crbn*$^{-/-}$ CD8$^+$ T cells was Myc dependent, we treated activated cells with a series of Myc:Max heterodimerization inhibitors[46] at the time of activation (Figure 5C-D). As expected, treatment with these Myc:Max disrupters blocked the induction of the Myc target gene *Odc1* in *Crbn*$^{-/-}$ CD8$^+$ T cells (Figure 5E), as well as that of the glutamine transporters *Slc38a1* and *Slc1a5* and the polyamine biosynthetic enzymes *Srm* and *Sms* (supplemental Figure 4C). Interestingly, the effector gene signature of activated *Crbn*$^{-/-}$ CD8$^+$ T cells, including *Tbx21*, *Eomes*, *Gzmb*, and *Ifng*, was also suppressed in a dose-dependent manner by treatment with these Myc:Max inhibitors (Figure 5F; supplemental 4D). Thus, the metabolic and T_E signatures of activated *Crbn*$^{-/-}$ CD8$^+$ T cells are Myc dependent.

Crbn deficiency augments T-cell activity in GVHD

IM compounds are associated with exacerbated GVHD toxicity in patients with multiple myeloma who undergo allogeneic hematopoietic cell transplantation,[47] which is most likely related to potentiated T_E-cell functions. Moreover, alloreactive T cells that drive GVHD are metabolically reprogrammed.[48] To assess the effects of *Crbn* deficiency on polyclonal T-cell activation in vivo in response to alloantigens, we used a lethal mouse model of GVHD, where lethally irradiated major histocompatibility complex–mismatched BALB/c (H2^d) recipients are reconstituted with donor-derived C57Bl/6 (H2^b) CD3$^+$ T-cell–depleted bone marrow.[49] After randomization, equal numbers of C57Bl/6 *Crbn*$^{+/+}$ and *Crbn*$^{-/-}$ T cells were transferred into lethally irradiated recipient BALB/c mice (Figure 6A). Notably, recipients receiving *Crbn*$^{-/-}$ T cells displayed a rapid loss in body weight and quickly succumbed to GVHD, compared with recipients receiving *Crbn*$^{+/+}$ T cells (Figure 6B; P = .017). Significantly higher percentages of CD4$^+$ and CD8$^+$ effector T cells expressing IFN-γ were evident in mice receiving *Crbn*$^{-/-}$ T cells 14 days after transplantation (Figure 6C), yet *Crbn*$^{-/-}$ and *Crbn*$^{+/+}$ donor cells had a similar number of T cells expressing the proinflammatory cytokine IL-17 (supplemental Figure 5A),

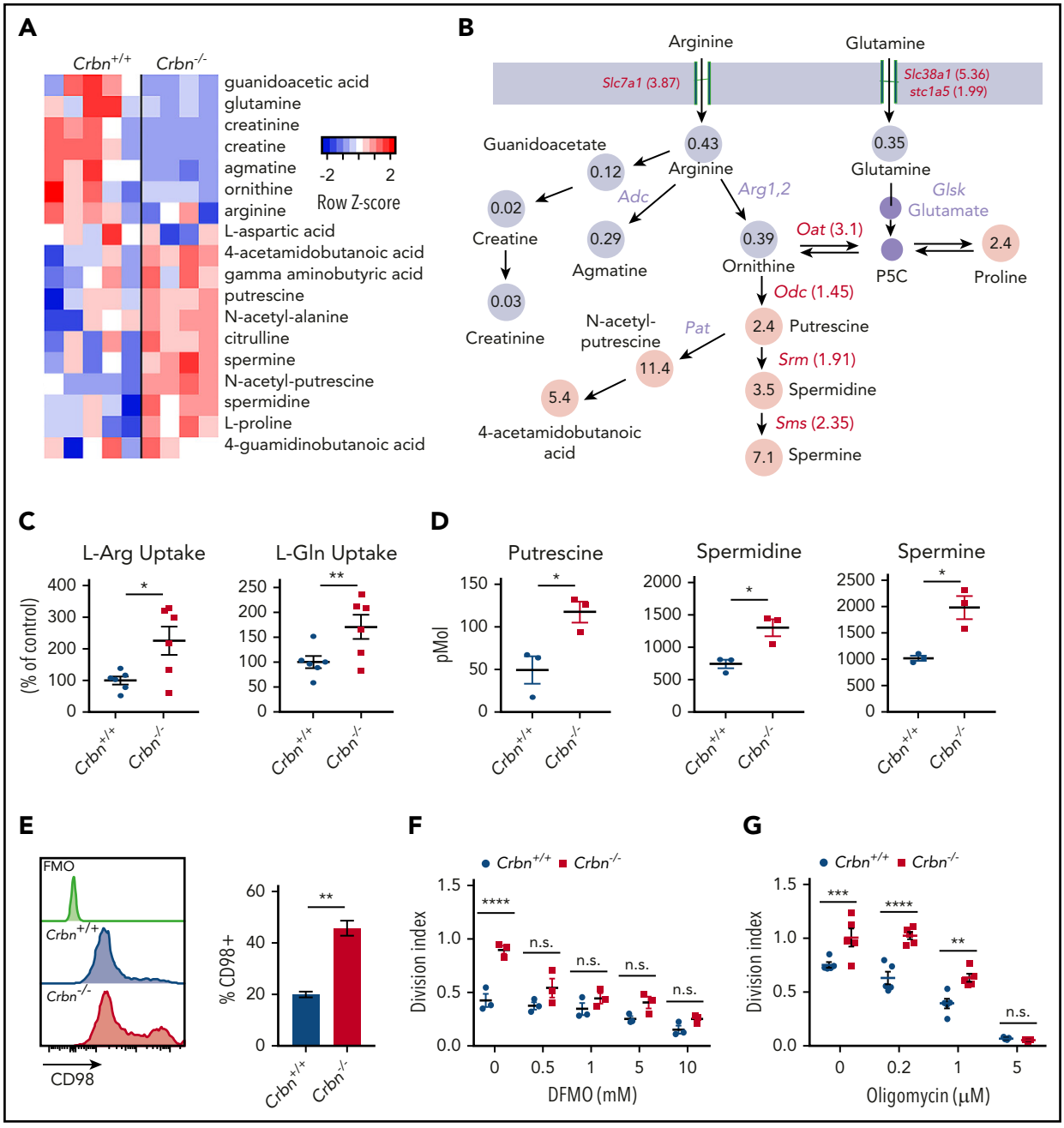

Figure 4. CRBN harnesses arginine and glutamine metabolism in activated CD8⁺ T cells. (A-B) Metabolomic LC-MS/MS analysis of 24-hour anti-CD3ε+anti-CD28–activated *Crbn*$^{+/+}$and *Crbn*$^{-/-}$ CD8⁺ T cells. (A) Heat map of metabolites that were significantly different and (B) the average fold change in arginine, glutamine, and proline metabolites. Gray indicates downregulated metabolites in the pathway, and pink denotes increased metabolites in the pathway. Fold change in mRNA levels for enzymes and transporters for each reaction are indicated. All enzymes and transporters were upregulated by the fold change indicated in *Crbn*$^{-/-}$ CD8⁺ T cells. Enzymes that were not assessed for differential expression are shown in lavender. (C) L-Arg and L-Glu uptake (% of control) by *Crbn*$^{+/+}$ and *Crbn*$^{-/-}$ CD8⁺ T cells after 24 hours of anti-CD3ε+anti-CD28 activation. (D) Intracellular putrescine, spermidine, and spermine levels measured by LC-MS/MS of activated *Crbn*$^{+/+}$and *Crbn*$^{-/-}$ CD8⁺ T cells (24 hours). (E) Flow cytometric analyses of CD98 expression in *Crbn*$^{+/+}$and *Crbn*$^{-/-}$ CD8⁺ T cells after anti-CD3ε+anti-CD28 stimulation for 24 hours. (F-G) *Crbn*$^{+/+}$ and *Crbn*$^{-/-}$ CD8⁺ T-cell proliferation after 72 hours of anti-CD3ε+anti-CD28 stimulation with cotreatment of α-difluoromethylornithine (5 mM; DFMO; F) or oligomycin (G). All results are representative of at least 2 independent experiments (excluding metabolomics analysis). n.s., not significant; *$P < .05$; ** $P < .01$; ***$P < .001$; ****$P < .0001$.

which can provoke tissue toxicity.[50] Moreover, the number of T cells producing another cytokine marker of acute GVHD,[51] IL-5 (supplemental Figure 5A), were similar on day 14 after bone marrow transplantation.

Histopathological analyses of skin, colon, and liver confirmed pathology consistent with GVHD[49] in mice receiving both *Crbn*$^{+/+}$ and *Crbn*$^{-/-}$ T cells (supplemental Figure 5B). Because GVHD can be influenced by altered lymphopenia-associated proliferation and activation,[28] T cells from *Crbn*$^{+/+}$ and *Crbn*$^{-/-}$ littermates were adoptively transferred into sublethally irradiated syngeneic mice. The division index of CD4⁺ and CD8⁺ T cells and splenocyte numbers were equally distributed in mice receiving *Crbn*$^{+/+}$ vs those receiving *Crbn*$^{-/-}$ T cells, suggesting

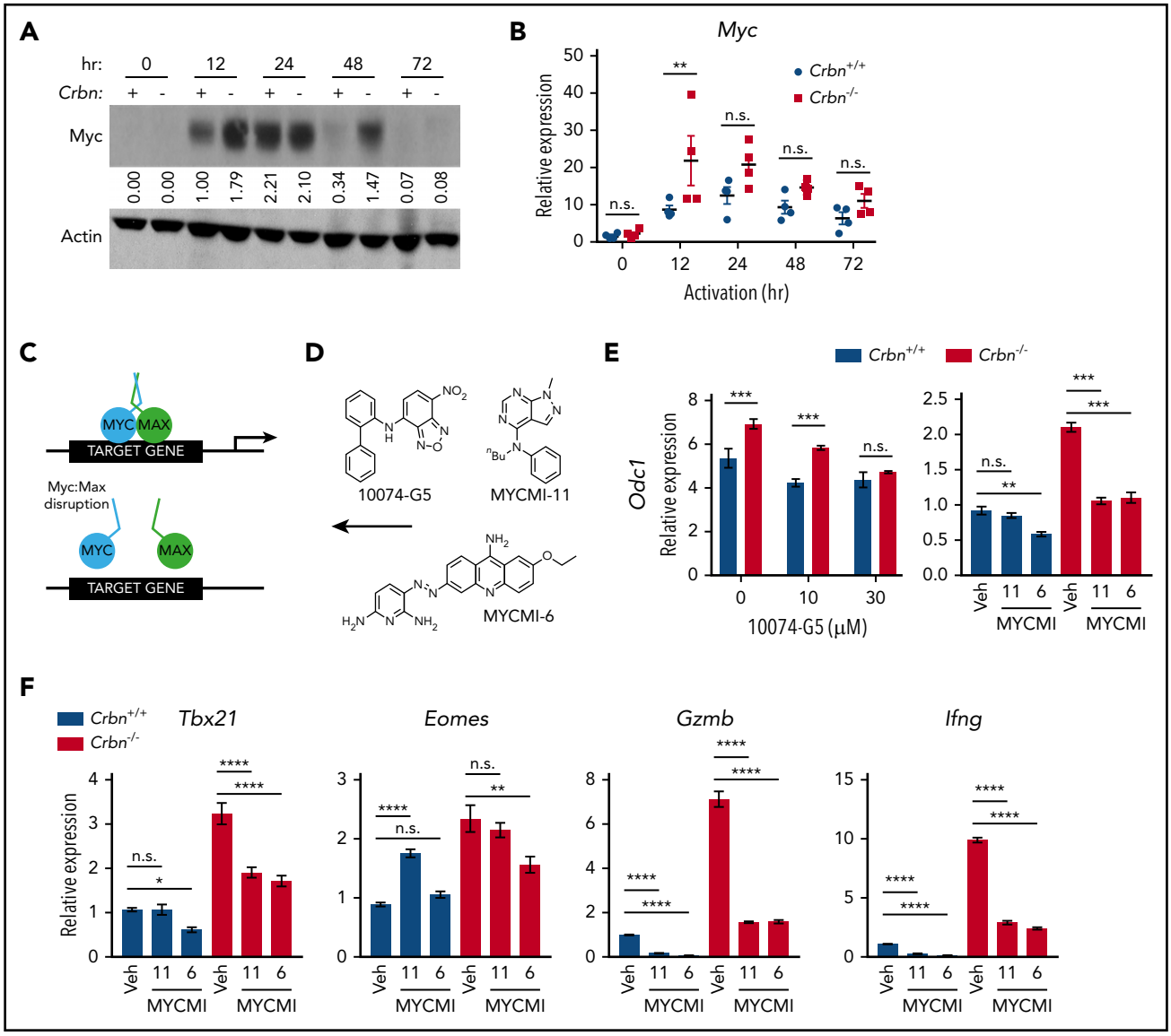

Figure 5. CRBN controls T_E phenotype by altering the dynamic regulation of MYC. (A) Myc protein levels in activated *Crbn*$^{+/+}$ and *Crbn*$^{-/-}$ T cells (denoted + and −) were determined by immunoblot analysis at the indicated intervals after stimulation with anti-CD3ε+anti-CD28. The expression shown is relative to levels of β-actin, and the data are representative of 4 independent experiments. Values indicate band density of the western blot. (B) *Myc* mRNA levels in *Crbn*$^{+/+}$ and *Crbn*$^{-/-}$ CD8$^+$ T cells after activation by anti-CD3ε+anti-CD28 for the times indicated. (C) Diagram of MYC:MAX pharmacological disruption and (D) the structures of 10074-G5, MYCMI-11, and MYCMI-6 MYC:MAX inhibitors used. (E-F) CD8$^+$ T cells were stimulated with anti-CD3ε+anti-CD28 for 24 hours, with or without cotreatment with the indicated doses of 10074-G5 or with 30 μM MYCMI-11 or MYCI-6 MYC/MAX dimerization inhibitors. Levels of *Odc1* (E), and the T_E signature genes *Tbx21*, *Eomes*, *Gzmb*, and *Ifng* transcripts in *Crbn*$^{+/+}$and *Crbn*$^{-/-}$ CD8$^+$ T cells (F). All results are representative of at least 2 independent experiments. n.s., not significant; *$P < .05$; **$P < .01$; ***$P < .001$; ****$P < .0001$.

no differences in persistence after homeostatic expansion (supplemental Figure 5C-F). Moreover, both populations of naïve T cells that proliferated in response to acute, transient lymphopenia acquired the characteristic conversion to a memory-like T-cell phenotype at the same rate[28] (supplemental Figure 5G-H).

In patients who undergo hematopoietic stem cell transplantation, the amount of activating protein 1 (AP-1), a leucine zipper transcription factor complex composed of c-Fos:c-Jun heterodimers, is an important determinant of GVHD severity.[52] In our work, GSEA for transcriptional drivers revealed enrichment of AP-1 transcriptional activity in activated *Crbn*$^{-/-}$ CD8$^+$ T cells (supplemental Figure 4A). One study has shown that extracellular-regulated kinase (ERK) activation, AP-1 induction, and expression of the activation marker CD69 are linked processes.[53] Moreover, MEK inhibitors selectively suppress alloreactivity and GVHD pathology.[54,55] Notably, activated *Crbn*$^{-/-}$ CD8$^+$ T cells had a 50% increase in total ERK1/2 vs *Crbn*$^{+/+}$ T cells (Figure 6D). Further, treatment with the selective MEK inhibitor PD98059 effectively suppressed the increases in total and phospho-ERK1/2 manifested in activated *Crbn*$^{-/-}$ CD8$^+$ T cells and completely abolished the high levels of Myc protein and mRNA and the effector genes *Tbx21*, *Eomes*, *Gzmb*, and *Ifng* in activated *Crbn*$^{-/-}$ T cells (Figure 6D-E). These findings are consistent with a model wherein CRBN harnesses an ERK1/2-to-AP-1/Myc pathway after activation of CD8$^+$ T cells to dampen T_E phenotypes.

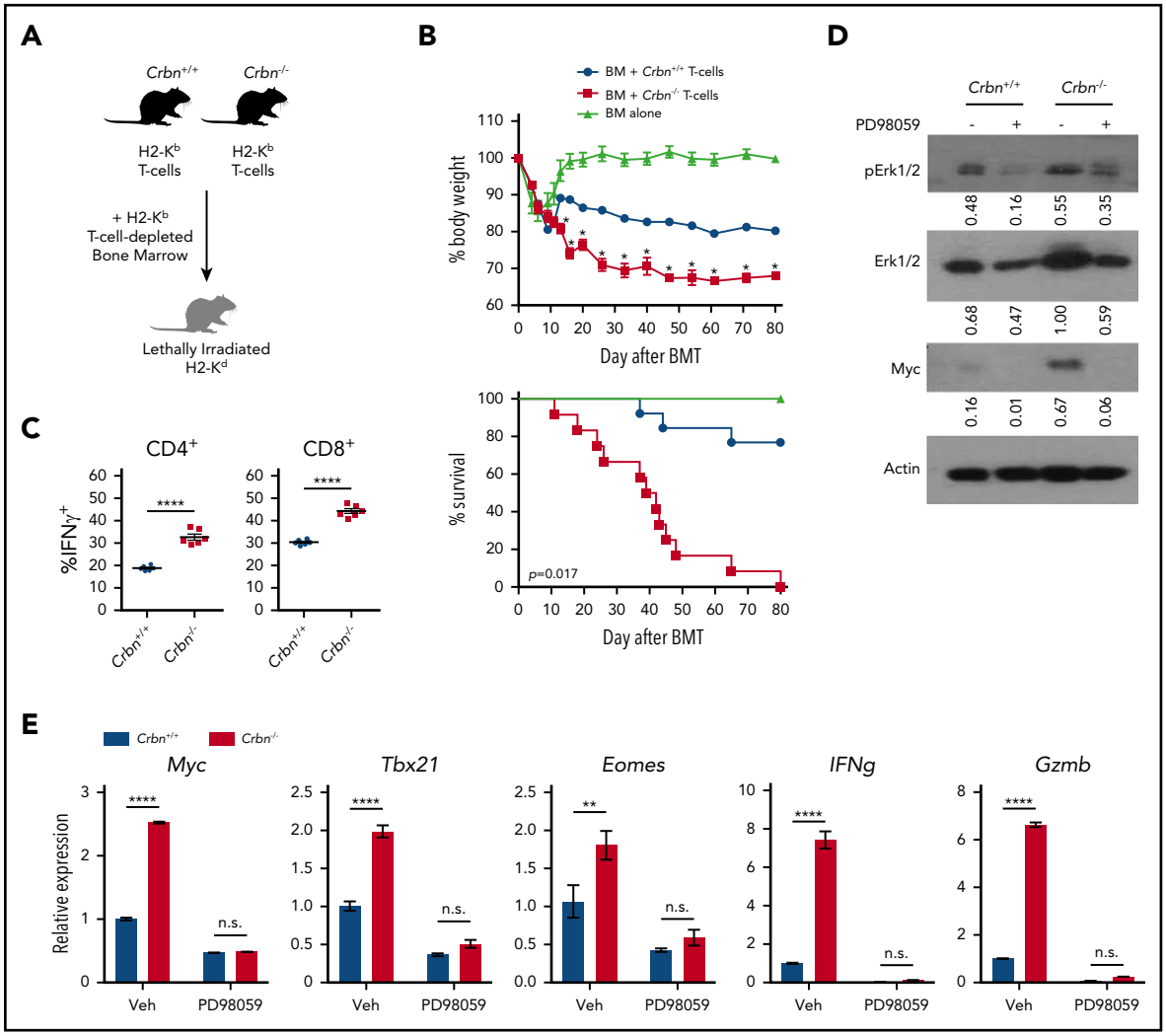

Figure 6. CRBN controls T_E phenotype and harnesses GVHD pathogenesis. (A) Schematic of GVHD experiments. (B) Effects of GVHD in a model of BALB/c mice receiving C57Bl/6 T-cell–depleted bone marrow, with and without *Crbn*$^{+/+}$ or *Crbn*$^{-/-}$ T cells (H2^{b}) after lethal body irradiation. The percentage of body weight (top) and survival (bottom) of recipient BALB/c H2^{d} mice was monitored at the indicated intervals. (C) The percentage of IFN-γ–producing CD4^{+} and CD8^{+} T cells in donor *Crbn*$^{+/+}$ or *Crbn*$^{-/-}$ T cells derived from the GVHD model after restimulation with phorbol myristate acetate and ionomycin ex vivo on day 14 after transplantation. (D) pERK1/2, total ERK1/2, and Myc protein levels, as determined by western blot analysis in *Crbn*$^{+/+}$ and *Crbn*$^{-/-}$ CD8^{+} T cells, with or without 25 μM PD98059 24 hours after activation with anti-CD3ε+anti-CD28. (E) qRT-PCR analysis of *Myc*, *Tbx21*, *Eomes*, *Ifng*, and *Gzmb* mRNA levels in *Crbn*$^{+/+}$ vs *Crbn*$^{-/-}$ CD8^{+} T cells 24 hours after activation with anti-CD3ε+anti-CD28$^{+/-}$ cotreatment with 25 μM PD98059. All results are representative of at least 2 independent experiments. n.s., not significant; *$P < .05$; **$P < .01$; ****$P < .0001$.

IM compounds induce MYC and MYC-dependent phenotypes in human CD8^{+} T cells

Putative mechanisms for IM compounds include dual activity via neosubstrate degradation and target binding interference, which would downregulate and upregulate IM target proteins, respectively.[10] Currently, there are no known endogenous proteins or pathways linked to the T-cell phenotypes provoked by IM compounds.[10] To test whether IM compounds affect the CRBN-MYC circuit, activated human CD4^{+} and CD8^{+} T cells from healthy human donors were treated with the IM compounds lenalidomide, pomalidomide, and CC-122 (avadomide). Similar to previous studies in which lenalidomide and pomalidomide were used,[56-59] treatment of human CD8^{+} T cells with avadomide[7] significantly increased IFN-γ secretion, especially in cells stimulated with low levels of anti-CD3ε and anti-CD28 (supplemental Figure 6A). All 3 IM compounds augmented the metabolism of activated CD8^{+} T cells, including increased OCR (Figure 7A) and ECAR (Figure 7B), and all 3 suppressed the levels of IKAROS in CD8^{+} T cells (supplemental Figure 6B). Notably, MYC protein levels in these T cells, as measured by mean fluorescence intensity (MFI), were significantly increased by treatment with the IM compounds (Figure 7C; supplemental Figure 6C). Further, the expression of CD98 (Figure 7D), glucose uptake, and cell size (Figure 7E) were also augmented in activated human CD8^{+} T cells after IM treatment (supplemental Table 5), and treatment-induced 2-NDBG uptake and cell size were effectively blocked by cotreatment with the MYC:MAX inhibitor 10074-G5 (Figure 7F; supplemental Table S5). Finally, CRISPR (clustered regularly interspaced short palindromic repeats)/cas9directed knockdown of *CRBN* expression in primary human CD8^{+} T cells provoked increases in *MYC* and *IFNg* expression after activation (Figure 7F; supplemental Figure 6D). Thus, IM compound treatment or CRBN knockdown in activated human CD8^{+} T cells drives a superior T_E phenotype that resembles mouse *Crbn*$^{-/-}$ CD8^{+} T cells.

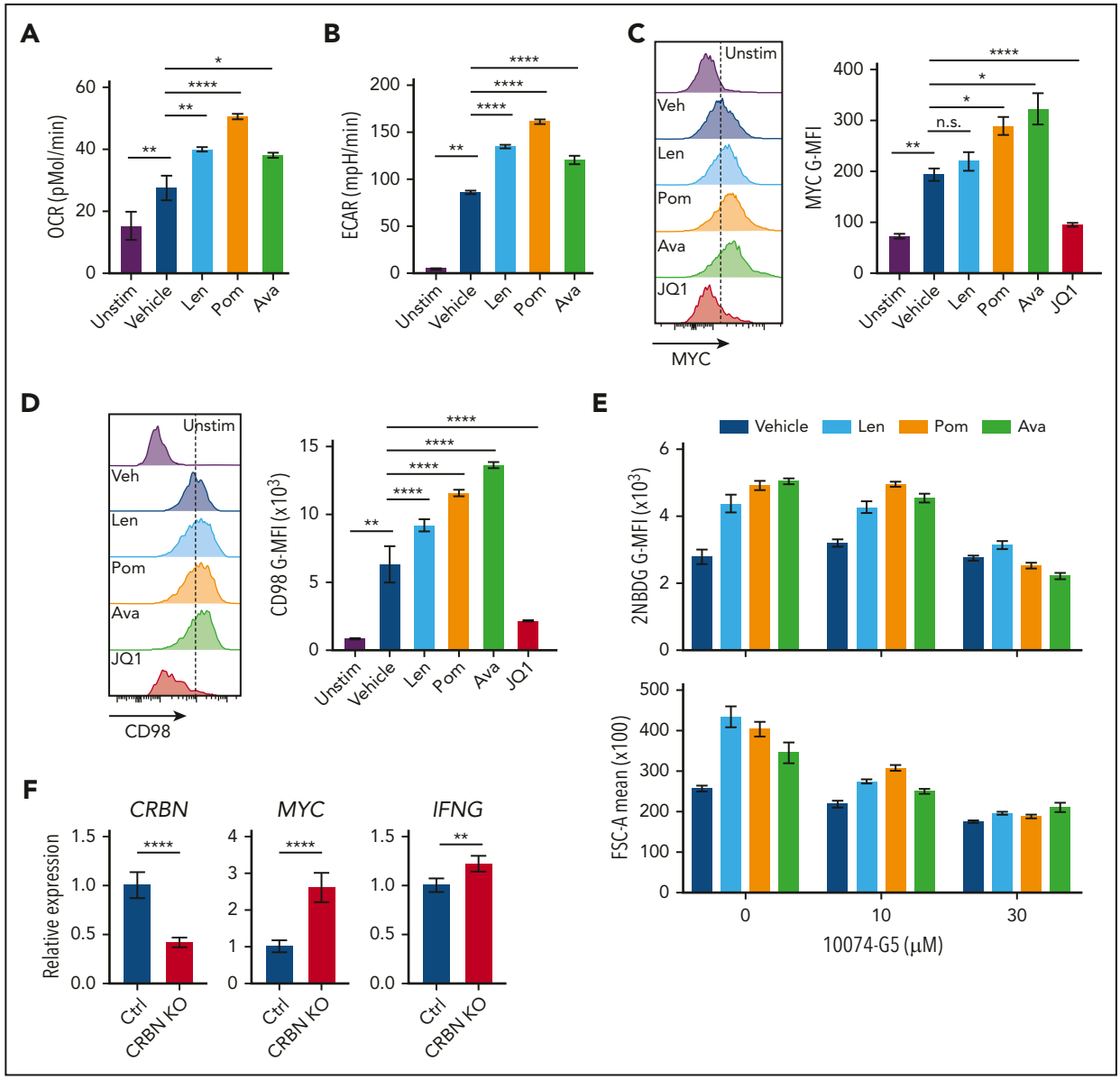

Figure 7. Targeting CRBN augments human CD8⁺ T-cell bioenergetics and MYC expression. OCRs (A) and ECARs (B) in activated human CD8⁺ T cells treated with vehicle or IM compounds for 5 days, as indicated, at a 10-μM dose of lenalidomide (Len), pomalidomide (Pom), and avadomide (Ava). (C) MYC protein levels in unstimulated (Unstim) and anti-CD3+anti-CD28–activated human CD8⁺ T cells treated with IM compounds (Len, Pom or Ava; 10 μM) for 5 days as detected by flow cytometry. JQ1 (a BET inhibitor) was used to show staining specificity for MYC in these experiments. (D) CD98 surface expression in activated human CD8⁺ T cells treated with IM compounds for 5 days. (E) Glucose uptake (top) and cell size (bottom) of activated (treated with anti-CD3+anti-CD28) human CD8⁺ T cells treated with IM compounds, with or without the MYC/MAX dimerization inhibitor 10074-G4, as measured using the fluorescent glucose analogue 2-NBDG (top) or forward scatter area (FSC-A, bottom) by flow cytometry. (F) Resting CD8⁺ T cells, enriched from healthy donor peripheral blood mononuclear cell (PBMCs), and complexed ribonucleoproteins (CRBN gRNAs+CAS9) were mixed with 4×10^6 CD8⁺ T cells, resuspended in primary cell solution, and nucleoporated. After nucleoporation, the cells were rested for 48 hours and then activated with anti-CD3+anti-CD28. After 5 days, the cells were assessed for levels of *CRBN*, *MYC*, and *IFNg* mRNA vs *B2M* transcripts by qRT-PCR. All results are representative of at least 2 independent experiments (excluding the CRISPR experiments). For statistical comparisons, see supplemental Table 5. n.s., not significant; *$P < .05$; **$P < .01$; ****$P < .0001$.

Discussion

Targeting CRBN in activated mouse and human CD8⁺ T cells, either via genetic means or through small-molecule treatment, generates a robust metabolic, hyperactive CD8⁺ T_E phenotype that has enhanced activity in a validated model of GVHD and enhanced antitumor activity in a syngeneic melanoma tumor model. These findings suggest that targeting CBRN would augment the antitumor activity of the immune checkpoint, tumor-infiltrating leukocytes, and/or chimeric antigen receptor–T-cell therapeutic strategies, but enhance the severity of GVHD in transplantation settings. In support of the latter, CD98 signaling[56] and anaplerosis of alloreactive T cells[57] have been implicated in GVHD severity, and these responses appear to be harnessed by CRBN.

CRBN has been reported to control metabolism in other cell types, by directing degradation of glutamine synthetase (GS)[60] via interactions with acetylated lysines of GS that are triggered by high intracellular glutamine concentrations and by CRBN-directed suppression of the activity of the α1 subunit of

AMP-activated protein kinase (*AMPKa1*),[61] a regulator of energy homeostasis. Further, CRBN binds to the CD147-SLC16A1 (MCT1) lactate transporter complex in multiple myeloma cells, and IM drug binding destabilizes this complex, contributing to its antineoplastic activity in this malignancy.[19]

Our studies established the striking finding that CRBN harnesses $CD8^+$ T-cell metabolism downstream of the MEK/ERK signaling pathway, which is necessary for the induction of Myc after TCR engagement. The control of Myc by CRBN is entirely novel and is highly significant in T-cell biology, as Myc functions as a master regulator of T-cell activation and metabolism[26] and also controls asymmetric division of T cells into effector vs memory cell fates.[62,63] Notably, Green and colleagues[26] have shown that Myc augments metabolism and enables the proliferation of $CD4^+$ and $CD8^+$ T cells via transcriptional reprogramming that includes induction of enzymes that direct glycolysis, glutaminolysis, and polyamine biosynthesis. Consistent with high Myc activity, *Crbn*-deficient activated mouse $CD8^+$ T cells and human $CD8^+$ T cells treated with IM compounds exhibit increased levels of MYC, and in T cells, this leads to enhanced nutrient uptake, NAD^+/NADH ratios, glycolytic rates, and basal and reserve capacity for OXPHOS. Further, MYC function is necessary to sustain the hypermetabolic phenotype of activated mouse and human $CD8^+$ T cells, as these are cancelled by treatment with validated inhibitors of MYC:MAX function.[46,64] Thus, a CRBN-MYC circuit controls the magnitude of antigen-specific activation of $CD8^+$ T cells and drives a hyperactive T_E-cell fate.

MYC expression is controlled by several means, including mRNA decay,[65] ubiquitin-mediated protein turnover by DDB1-Cul4A-TRUSS[66,67] (evident using the EGFP-MYC reporter), and microRNA and long noncoding RNA regulation,[68-70] transcription,[71] and translation.[72] Thus, the control of *Myc* mRNA and protein levels in activated T cells and by CRBN in this context, is likely to be very complex. What is known is that *Myc* mRNA induction involves an increase in both transcription initiation and a release from an elongation block.[73] Intriguingly, translational regulation of Myc also includes a polyamine-directed pathway,[74] which we have shown is highly elevated in *Crbn*-deficient T cells that rely on polyamine biosynthesis to sustain their hyperactive phenotype. In our study, a primary regulator of *Myc* mRNA and protein expression was MEK/ERK signaling, which is interesting, given the established roles of MEK/ERK activation in the control of both acute and chronic GVHD.[54,55,75] Precisely how CRBN harnesses MEK/ERK1 signaling and how this then sustains high levels of Myc expression in activated $CD8^+$ T cells is not yet clear, but it represents an important area for future investigation, along with studies that resolve how TCR signaling dynamically controls the expression of CRBN itself.

Notably, T-bet expression is increased 7- to 12-fold in activated $Crbn^{-/-}$ $CD8^+$ T cells, which is consistent with their cytokine production profile, gene signature, and metabolic phenotypes. Germane to our study, high T-bet and its induction of IFN-γ are critical determinants of acute GVHD[50] and suggest that impaired CRBN function contributes to poor clinical outcomes. This, and the augmented antitumor phenotype of $Crbn^{-/-}$ $CD8^+$ T cells, suggests the CRBN-MEK/ERK-Myc circuit (supplemental Figure 7), which augments, sustains, and drives an antigen-specific T-cell phenotype, could have far-reaching clinical applications. Important future translational studies include those that will assess the anticancer efficacy of targeting CRBN in maintenance of graft versus leukemia, and in improving the efficacy of a broad spectrum of immune checkpoint and adoptive cell therapies.

Acknowledgments

The authors thank Dalia Ercan; the staffs of the Proteomics and Metabolomics, Flow Cytometry, Molecular Genomics, Cancer Informatics, and Chemical Biology Cores of the Moffitt Cancer Center; the Moffitt/University of South Florida Comparative Medicine Program; and the University of South Florida (USF) Health Lisa Muma Weitz Laboratory for Advanced Microscopy and Cell Imaging.

This work was supported by a National Natural Science Foundation of China grant (81702268) (Y.H.); a Natural Science Foundation of Tianjin grant (18JCYBJC93400) (Y.H.); a Sponsored Research Agreement with Celgene Corporation (N.J.L., P.K.E.-B.); the Cortner-Couch Endowed Chair for Cancer Research of the USF School of Medicine (J.L.C.); funds from Lesa France Kennedy (J.L.C.); a Leukemia and Lymphoma Society-Specialized Center of Research (LLS-SCOR) grant (J.L.C.); National Institutes of Health, National Cancer Institute (NCI) Center Core Support grant (P30-CA076292); funds from the State of Florida to the Moffitt Cancer Center and Research Institute; the NCI in conjunction with a Career Enhancement Award from the Moffitt Skin Cancer Specialized Programs of Research Excellence (SPORE) grant (P50CA168536) (P.K.E.-B.); a NCI Research Specialist award (R50CA211447) (H.R.L.); an NCI National Research Service Award (F32CA203217) (M.R.F.); and a research grant from Celgene Corporation to the Moffitt Cancer Center and Research Institute.

Authorship

Contribution: R.S.H., M.S.B., and Y.H. contributed equally to the discovery of the new concepts presented in this manuscript; R.S.H., J.L.C., and P.K.E.-B. designed the research plan, performed the experiments, analyzed and interpreted the data, and prepared the manuscript; M.R.F., A.A.A., W.E.G., C.Y., A.Y.A., S.C., J.M.M., A.W.M., J.M.R.B., C.M.C., and L.Y. performed the experiments, analyzed and interpreted the data, and prepared the figures; J.M.K., L.N.D., and T.J.G. performed the metabolomics studies; X.-Z.Y. designed the experiments and assisted with the studies of GVHD; J.F. assisted with the GVHD model design and data analysis; M.A. and S.Y.Y. synthesized the chemicals; H.R.L. and N.J.L. provided concept design for synthesis of key chemical reagents, interpreted the results, and helped in the preparation of the article; S.R. and R.J.G. participated in concept design and provided specialized research expertise in metabolomics; Y.H. performed the GVHD experiments; K.J. and J.M. provided the pathology analysis for the GVHD model; X.R. provided financial support through an integrated Moffitt research alliance; A.M.R. provided key reagents and expertise; J.L.C. and P.K.E.-B. shared equally in manuscript preparation and designed the research plan, performed the data analysis, and interpreted the results, and took responsibility for all aspects of the work; and all authors reviewed and agreed to the publication of the data.

Conflict-of-interest disclosure: J.M.M. was a salaried employee of Celgene Corporation, but was a graduate student in the Cancer Biology PhD program at the time of her involvement in this study. N.J.L., H.R.L., P.K.E.-B., and the Moffitt Cancer Center and Research Institute received payment from licensing unrelated technology to Celgene Corporation and have an appropriate conflict-of-interest management plan. The remaining authors declare no competing financial interests.

ORCID profiles: R.S.H., 0000-0003-0472-7517; M.R.F., 0000-0002-2017-9576; J.M.R.B., 0000-0003-2831-1428; L.Y., 0000-0002-8578-7564; S.R., 0000-0003-1066-6132; R.J.G., 0000-0002-8888-7747; N.J.L., 0000-0003-1129-2558; H.R.L., 0000-0002-9263-7775; J.F., 0000-0003-1500-5405; J.M.K., 0000-0002-3818-1762; J.M., 0000-0002-0332-0224; K.J., 0000-0001-8531-7813; T.J.G., 0000-0003-1623-009X.

The current affiliation for M.A. is the Department of Chemistry Quaid-e-Azam University, Islamabad, Pakistan.Correspondence: John L. Cleveland, Department of Tumor Biology, H. Lee Moffitt Cancer Center and Research Institute, 12902 Magnolia Dr, Tampa, FL 33612; e-mail: john.cleveland@moffitt.org.

Footnotes

Submitted 11 September 2019; accepted 20 April 2020; prepublished online on *Blood* First Edition 13 May 2020. DOI 10.1182/blood.2019003257.

*R.S.H., M.S.B., and Y.H. contributed equally to this study.

The data reported in this article have been deposited in the Gene Expression Omnibus database (accession number GSE81725).

The online version of this article contains a data supplement.

The publication costs of this article were defrayed in part by page charge payment. Therefore, and solely to indicate this fact, this article is hereby marked "advertisement" in accordance with 18 USC section 1734.

REFERENCES

1. Higgins JJ, Pucilowska J, Lombardi RQ, Rooney JP. A mutation in a novel ATP-dependent Lon protease gene in a kindred with mild mental retardation. *Neurology*. 2004;63(10):1927-1931.

2. Ito T, Ando H, Suzuki T, et al. Identification of a primary target of thalidomide teratogenicity. *Science*. 2010;327(5971):1345-1350.

3. Dimopoulos M, Spencer A, Attal M, et al; Multiple Myeloma (010) Study Investigators. Lenalidomide plus dexamethasone for relapsed or refractory multiple myeloma. *N Engl J Med*. 2007;357(21):2123-2132.

4. Weber DM, Chen C, Niesvizky R, et al; Multiple Myeloma (009) Study Investigators. Lenalidomide plus dexamethasone for relapsed multiple myeloma in North America. *N Engl J Med*. 2007;357(21):2133-2142.

5. Chanan-Khan A, Miller KC, Musial L, et al. Clinical efficacy of lenalidomide in patients with relapsed or refractory chronic lymphocytic leukemia: results of a phase II study. *J Clin Oncol*. 2006;24(34):5343-5349.

6. Yang Y, Shaffer AL III, Emre NC, et al. Exploiting synthetic lethality for the therapy of ABC diffuse large B cell lymphoma. *Cancer Cell*. 2012;21(6):723-737.

7. Hagner PR, Man HW, Fontanillo C, et al. CC-122, a pleiotropic pathway modifier, mimics an interferon response and has antitumor activity in DLBCL. *Blood*. 2015;126(6):779-789.

8. List A, Kurtin S, Roe DJ, et al. Efficacy of lenalidomide in myelodysplastic syndromes. *N Engl J Med*. 2005;352(6):549-557.

9. Talati C, Sallman D, List A. Lenalidomide: myelodysplastic syndromes with del(5q) and beyond. *Semin Hematol*. 2017;54(3):159-166.

10. Fischer ES, Böhm K, Lydeard JR, et al. Structure of the DDB1-CRBN E3 ubiquitin ligase in complex with thalidomide. *Nature*. 2014;512(7512):49-53.

11. Petzold G, Fischer ES, Thomä NH. Structural basis of lenalidomide-induced CK1α degradation by the CRL4(CRBN) ubiquitin ligase. *Nature*. 2016;532(7597):127-130.

12. Chamberlain PP, Lopez-Girona A, Miller K, et al. Structure of the human Cereblon-DDB1-lenalidomide complex reveals basis for responsiveness to thalidomide analogs. *Nat Struct Mol Biol*. 2014;21(9):803-809.

13. Gopalakrishnan R, Matta H, Tolani B, Triche T Jr., Chaudhary PM. Immunomodulatory drugs target IKZF1-IRF4-MYC axis in primary effusion lymphoma in a cereblon-dependent manner and display synergistic cytotoxicity with BRD4 inhibitors. *Oncogene*. 2016;35(14):1797-1810.

14. Lu G, Middleton RE, Sun H, et al. The myeloma drug lenalidomide promotes the cereblon-dependent destruction of Ikaros proteins. *Science*. 2014;343(6168):305-309.

15. Winter GE, Buckley DL, Paulk J, et al. Phthalimide conjugation as a strategy for in vivo target protein degradation. *Science*. 2015;348(6241):1376-1381.

16. O'Brien S, Thomas RM, Wertheim GB, Zhang F, Shen H, Wells AD. Ikaros imposes a barrier to CD8+ T cell differentiation by restricting autocrine IL-2 production. *J Immunol*. 2014;192(11):5118-5129.

17. Harker N, Naito T, Cortes M, et al. The CD8alpha gene locus is regulated by the Ikaros family of proteins. *Mol Cell*. 2002;10(6):1403-1415.

18. Krönke J, Udeshi ND, Narla A, et al. Lenalidomide causes selective degradation of IKZF1 and IKZF3 in multiple myeloma cells. *Science*. 2014;343(6168):301-305.

19. Eichner R, Heider M, Fernández-Sáiz V, et al. Immunomodulatory drugs disrupt the cereblon-CD147-MCT1 axis to exert antitumor activity and teratogenicity. *Nat Med*. 2016;22(7):735-743.

20. Kang JA, Park SH, Jeong SP, et al. Epigenetic regulation of Kcna3-encoding Kv1.3 potassium channel by cereblon contributes to regulation of CD4+ T-cell activation. *Proc Natl Acad Sci USA*. 2016;113(31):8771-8776.

21. Buck MD, O'Sullivan D, Klein Geltink RI, et al. Mitochondrial Dynamics Controls T Cell Fate through Metabolic Programming. *Cell*. 2016;166(1):63-76.

22. Michalek RD, Rathmell JC. The metabolic life and times of a T-cell. *Immunol Rev*. 2010;236(1):190-202.

23. Ho PC, Bihuniak JD, Macintyre AN, et al. Phosphoenolpyruvate Is a Metabolic Checkpoint of Anti-tumor T Cell Responses. *Cell*. 2015;162(6):1217-1228.

24. Palmer CS, Hussain T, Duette G, et al. Regulators of Glucose Metabolism in CD4$^+$ and CD8$^+$ T Cells. *Int Rev Immunol*. 2016;35(6):477-488.

25. Chang CH, Pearce EL. Emerging concepts of T cell metabolism as a target of immunotherapy. *Nat Immunol*. 2016;17(4):364-368.

26. Wang R, Dillon CP, Shi LZ, et al. The transcription factor Myc controls metabolic reprogramming upon T lymphocyte activation. *Immunity*. 2011;35(6):871-882.

27. Rajadhyaksha AM, Ra S, Kishinevsky S, et al. Behavioral characterization of cereblon forebrain-specific conditional null mice: a model for human non-syndromic intellectual disability. *Behav Brain Res*. 2012;226(2):428-434.

28. Cheung KP, Yang E, Goldrath AW. Memory-like CD8+ T cells generated during homeostatic proliferation defer to antigen-experienced memory cells. *J Immunol*. 2009;183(5):3364-3372.

29. Messaoudi I, Warner J, Nikolich-Zugich D, Fischer M, Nikolich-Zugich J. Molecular, cellular, and antigen requirements for development of age-associated T cell clonal expansions in vivo. *J Immunol*. 2006;176(1):301-308.

30. Sullivan BM, Juedes A, Szabo SJ, von Herrath M, Glimcher LH. Antigen-driven effector CD8 T cell function regulated by T-bet. *Proc Natl Acad Sci USA*. 2003;100(26):15818-15823.

31. Intlekofer AM, Takemoto N, Wherry EJ, et al. Effector and memory CD8+ T cell fate coupled by T-bet and eomesodermin [*Nat Immunol*. 2006 Jan;7(1):113]. *Nat Immunol*. 2005;6(12):1236-1244.

32. Zheng Y, Delgoffe GM, Meyer CF, Chan W, Powell JD. Anergic T cells are metabolically anergic. *J Immunol*. 2009;183(10):6095-6101.

33. Stein LR, Imai S. The dynamic regulation of NAD metabolism in mitochondria. *Trends Endocrinol Metab*. 2012;23(9):420-428.

34. Hogquist KA, Jameson SC, Heath WR, Howard JL, Bevan MJ, Carbone FR. T cell receptor antagonist peptides induce positive selection. *Cell*. 1994;76(1):17-27.

35. Mareeva T, Lebedeva T, Anikeeva N, Manser T, Sykulev Y. Antibody specific for the peptide.major histocompatibility complex. Is it T cell receptor-like? *J Biol Chem*. 2004;279(43):44243-44249.

36. Sukumar M, Liu J, Ji Y, et al. Inhibiting glycolytic metabolism enhances CD8+ T cell memory and antitumor function. *J Clin Invest*. 2013;123(10):4479-4488.

37. Chang CH, Curtis JD, Maggi LB Jr., et al. Posttranscriptional control of T cell effector function by aerobic glycolysis. *Cell*. 2013;153(6):1239-1251.

38. Nakanishi S, Cleveland JL. Targeting the polyamine-hypusine circuit for the prevention and treatment of cancer. *Amino Acids*. 2016;48(10):2353-2362.

39. Cui Z, Zharikov S, Xia SL, et al. Molecular cloning, characterization, and chromosomal assignment of porcine cationic amino acid transporter-1. *Genomics*. 2005;85(3):352-359.

40. Bröer A, Rahimi F, Bröer S. Deletion of amino acid transporter ASCT2 (SLC1A5) reveals an essential role for transporters SNAT1 (SLC38A1) and SNAT2 (SLC38A2) to sustain glutaminolysis in cancer cells. *J Biol Chem*. 2016;291(25):13194-13205.

41. Cantor J, Slepak M, Ege N, Chang JT, Ginsberg MH. Loss of T cell CD98 H chain specifically ablates T cell clonal expansion and protects from autoimmunity. *J Immunol*. 2011; 187(2):851-860.

42. Maeda T, Wakasawa T, Shima Y, Tsuboi I, Aizawa S, Tamai I. Role of polyamines derived from arginine in differentiation and proliferation of human blood cells. *Biol Pharm Bull*. 2006;29(2):234-239.

43. Menk AV, Scharping NE, Rivadeneira DB, et al. 4-1BB costimulation induces T cell mitochondrial function and biogenesis enabling cancer immunotherapeutic responses. *J Exp Med*. 2018;215(4):1091-1100.

44. Stine ZE, Walton ZE, Altman BJ, Hsieh AL, Dang CV. MYC, Metabolism, and Cancer. *Cancer Discov*. 2015;5(10):1024-1039.

45. Nilsson JA, Keller UB, Baudino TA, et al. Targeting ornithine decarboxylase in Myc-induced lymphomagenesis prevents tumor formation. *Cancer Cell*. 2005;7(5):433-444.

46. Castell A, Yan Q, Fawkner K, et al. A selective high affinity MYC-binding compound inhibits MYC:MAX interaction and MYC-dependent tumor cell proliferation. *Sci Rep*. 2018;8(1): 10064.

47. Alsina M, Becker PS, Zhong X, et al; Resource for Clinical Investigation in Blood and Marrow Transplantation. Lenalidomide maintenance for high-risk multiple myeloma after allogeneic hematopoietic cell transplantation. *Biol Blood Marrow Transplant*. 2014;20(8):1183-1189.

48. Nguyen HD, Chatterjee S, Haarberg KM, et al. Metabolic reprogramming of alloantigen-activated T cells after hematopoietic cell transplantation. *J Clin Invest*. 2016;126(4): 1337-1352.

49. Valenzuela JO, Iclozan C, Hossain MS, et al. PKCtheta is required for alloreactivity and GVHD but not for immune responses toward leukemia and infection in mice. *J Clin Invest*. 2009;119(12):3774-3786.

50. Fu J, Wang D, Yu Y, et al. T-bet is critical for the development of acute graft-versus-host disease through controlling T cell differentiation and function. *J Immunol*. 2015;194(1): 388-397.

51. Imoto S, Oomoto Y, Murata K, et al. Kinetics of serum cytokines after allogeneic bone marrow transplantation: interleukin-5 as a potential marker of acute graft-versus-host disease. *Int J Hematol*. 2000;72(1):92-97.

52. Trop-Steinberg S, Azar Y, Bringer R, Or R. Myc and AP-1 expression in T cells and T-cell activation in patients after hematopoietic stem cell transplantation. *Clin Exp Med*. 2015;15(2): 189-203.

53. Shan X, Balakir R, Criado G, et al. Zap-70-independent Ca(2+) mobilization and Erk activation in Jurkat T cells in response to T-cell antigen receptor ligation. *Mol Cell Biol*. 2001; 21(21):7137-7149.

54. Shindo T, Kim TK, Benjamin CL, Wieder ED, Levy RB, Komanduri KV. MEK inhibitors selectively suppress alloreactivity and graft-versus-host disease in a memory stage-dependent manner. *Blood*. 2013;121(23): 4617-4626.

55. Lu SX, Alpdogan O, Lin J, et al. STAT-3 and ERK 1/2 phosphorylation are critical for T-cell alloactivation and graft-versus-host disease. *Blood*. 2008;112(13):5254-5258.

56. Nishio Y, Fujino M, Cai S, et al. Impaired CD98 signaling protects against graft-versus-host disease by increasing regulatory T cells. *Transpl Immunol*. 2016;35:34-39.

57. Glick GD, Rossignol R, Lyssiotis CA, et al. Anaplerotic metabolism of alloreactive T cells provides a metabolic approach to treat graft-versus-host disease. *J Pharmacol Exp Ther*. 2014;351(2):298-307.

58. Jo S, Lee KH, Song S, Jung YK, Park CS. Identification and functional characterization of cereblon as a binding protein for large-conductance calcium-activated potassium channel in rat brain. *J Neurochem*. 2005;94(5): 1212-1224.

59. Higgins JJ, Hao J, Kosofsky BE, Rajadhyaksha AM. Dysregulation of large-conductance Ca2+-activated K+ channel expression in nonsyndromal mental retardation due to a cereblon p.R419X mutation. *Neurogenetics*. 2008;9(3):219-223.

60. Nguyen TV, Lee JE, Sweredoski MJ, et al. Glutamine triggers acetylation-dependent degradation of glutamine synthetase via the thalidomide receptor cereblon. *Mol Cell*. 2016;61(6):809-820.

61. Lee KM, Jo S, Kim H, Lee J, Park CS. Functional modulation of AMP-activated protein kinase by cereblon. *Biochim Biophys Acta*. 2011;1813(3):448-455.

62. Verbist KC, Guy CS, Milasta S, et al. Metabolic maintenance of cell asymmetry following division in activated T lymphocytes. *Nature*. 2016;532(7599):389-393.

63. Pollizzi KN, Sun IH, Patel CH, et al. Asymmetric inheritance of mTORC1 kinase activity during division dictates CD8(+) T cell differentiation. *Nat Immunol*. 2016;17(6):704-711.

64. Clausen DM, Guo J, Parise RA, et al. In vitro cytotoxicity and in vivo efficacy, pharmacokinetics, and metabolism of 10074-G5, a novel small-molecule inhibitor of c-Myc/Max dimerization. *J Pharmacol Exp Ther*. 2010; 335(3):715-727.

65. Bernstein PL, Herrick DJ, Prokipcak RD, Ross J. Control of c-myc mRNA half-life in vitro by a protein capable of binding to a coding region stability determinant. *Genes Dev*. 1992;6(4): 642-654.

66. Choi SH, Wright JB, Gerber SA, Cole MD. Myc protein is stabilized by suppression of a novel E3 ligase complex in cancer cells. *Genes Dev*. 2010;24(12):1236-1241.

67. Liu H, Lu W, He H, et al. Inflammation-dependent overexpression of c-Myc enhances $CRL4^{DCAF4}$ E3 ligase activity and promotes ubiquitination of ST7 in colitis-associated cancer. *J Pathol*. 2019;248(4):464-475.

68. Amy CM, Bartholomew JC. Regulation of N-myc transcript stability in human neuroblastoma and retinoblastoma cells. *Cancer Res*. 1987;47(23):6310-6314.

69. Clement JQ, Wilkinson MF. Rapid induction of nuclear transcripts and inhibition of intron decay in response to the polymerase II inhibitor DRB. *J Mol Biol*. 2000;299(5):1179-1191.

70. Dorsett Y, McBride KM, Jankovic M, et al. MicroRNA-155 suppresses activation-induced cytidine deaminase-mediated Myc-Igh translocation. *Immunity*. 2008;28(5):630-638.

71. Liu J, Levens D. Making myc. *Curr Top Microbiol Immunol*. 2006;302:1-32.

72. Grzmil M, Hemmings BA. Translation regulation as a therapeutic target in cancer. *Cancer Res*. 2012;72(16):3891-3900.

73. Lindsten T, June CH, Thompson CB. Multiple mechanisms regulate c-myc gene expression during normal T cell activation. *EMBO J*. 1988; 7(9):2787-2794.

74. Liu L, Rao JN, Zou T, et al. Polyamines regulate c-Myc translation through Chk2-dependent HuR phosphorylation. *Mol Biol Cell*. 2009; 20(23):4885-4898.

75. Allen JL, Fore MS, Wooten J, et al. B cells from patients with chronic GVHD are activated and primed for survival via BAFF-mediated pathways. *Blood*. 2012;120(12):2529-2536.